J. Ocean Eng. Mar. Energy (2017) 3:385–394
DOI 10.1007/s40722-017-0097-3

RESEARCH ARTICLE

Experiments on higher-order and degenerate Akhmediev breather-type rogue water waves

Amin Chabchoub[1,2,3] · **Takuji Waseda**[2] · **Bertrand Kibler**[4] · **Nail Akhmediev**[5]

Received: 1 April 2017 / Accepted: 31 July 2017 / Published online: 31 August 2017

Abstract A possible mechanism that is responsible for the occurrence of rogue waves in the ocean is the Benjamin–Feir instability or modulation instability. The deterministic framework that describes this latter instability of Stokes waves in deep water is provided by the family of Akhmediev breather (AB) solutions of the nonlinear Schrödinger equation (NLS). It is indeed very convenient to use these exact pulsating envelopes particularly for laboratory experiments, since they allow to generate extreme waves at any location in space at any instant of time. As such, using this framework is more advantageous compared to the classical initialization of the unstable wave dynamics from a three wave system (main wave frequency and one pair of unstable sidebands). In this work, we report an experimental study on higher-order AB hydrodynamics that describe a higher-order stage of modulation instability, namely, starting from five wave systems (main wave frequency and two pairs of unstable sidebands). The corresponding laboratory experiments, that have been conducted in a large water wave facility, confirm the NLS wave dynamics forecast while boundary element method-based numerical wave tank simulations show a very good agreement with the experimental data.

Keywords Nonlinear waves · Breathers · Rogue waves · Boundary element method · Numerical wave tank

✉ Amin Chabchoub
amin.chabchoub@aalto.fi

1 Department of Mechanical Engineering, Aalto University, 02150 Espoo, Finland

2 Graduate School of Frontier Sciences, The University of Tokyo, Kashiwa, Chiba 277-8561, Japan

3 School of Civil Engineering, The University of Sydney, Sydney, NSW 2006, Australia

4 Laboratoire Interdisciplinaire Carnot de Bourgogne UMR6303 CNRS/Université de Bourgogne Franche-Comté, 21078 Dijon, France

5 Optical Sciences Group, Research School of Physics and Engineering, the Australian National University, Canberra, ACT 2600, Australia

1 Introduction

The modulation instability (MI) is known to be a universal mechanism that describes the disintegration of periodically perturbed wave trains in deep-water and that is responsible for the emergence of extreme water wave localizations (Benjamin and Feir 1967; Zakharov and Ostrovsky 2009). Since the 1960s significant progress has been made in this field of research, that includes several experimental studies in different physical media (Benjamin and Hasselmann 1967; Tulin and Waseda 1999; Tai et al. 1986). Indeed, MI has been suggested to provide an explanation for ocean rogue waves which suddenly appear and cause severe damages to ships and offshore structures (Kharif and Pelinovsky 2003; Kharif et al. 2009). The MI process is initiated when two small-amplitude sidebands of the unstable frequency range, located symmetrically around the main carrier frequency are spontaneously excited. As a result, a periodic focusing of the field with the following return to the initial state of constant amplitude wave occurs. In the spectral domain, this corresponds to formation of a triangular cascade and successive return to the initial wave field, consisting of single carrier frequency.

This fundamental process can be described within the framework of the nonlinear Schrödinger equation (NLS) (Zakharov 1968). In fact, for each unstable modulation frequency, one can assign an exact Akhmediev breather (AB) solution (Akhmediev et al. 1985; Akhmediev and Korneev

1986; Akhmediev et al. 1987) to describe the whole spatiotemporal unstable wave field dynamics (Wetzel et al. 2011). When studying the MI in laboratory environments, it turns out that breather description can be very useful when considering the excitation of extreme events (Dudley et al. 2009; Kibler et al. 2010; Chabchoub et al. 2011, 2014). Lately, it has been shown that breathers can indeed persist in sea state configurations (Chabchoub 2016), thus, proving its importance in the study of unidirectional extreme seas. Furthermore, recent studies also emphasized the significance of these pulsating solutions for sea keeping tests (Onorato et al. 2013) as well as for developing standards for ships and marine offshore structures (Bitner-Gregersen and Gramstad 2015).

On the other hand, the MI process can be much more complex when initial conditions are beyond a simple cosine-type perturbation of Stokes waves. In fact, MI can be initiated with five frequencies (carrier wave frequency and two pairs of unstable sidebands) or more. The corresponding solutions that model this type of instability dynamics are referred to as higher-order ABs (Akhmediev et al. 1985; Akhmediev 2012; Frisquet et al. 2014; Kibler et al. 2015). These regimes have higher amplitude amplification factors than three. Thus, the modeled waves are expected to be very steep.

Here, we investigate experimentally the dynamics of such higher-order ABs in a water wave facility (laboratory and numerical data). We find that both numerical and laboratory data are in very good agreement demonstrating that the NLS provides a practically good prediction of wave dynamics. Section 2 is devoted to describing the MI-AB formalism. In Sect. 3, the numerical scheme as well as the experimental set-up are described while Sects. 4 and 5 provide details of the laboratory and numerical results, respectively. Finally, the results are discussed in Sect. 6 while a perspective research is presented in the last conclusive Sect. 7.

2 Modulation instability and Akhmediev breather formalism

A dimensionless form of the time-NLS that is the basic governing equation for description of ocean wave dynamics in deep-water conditions, can be represented as

$$\mathrm{i}\,\psi_\xi + \frac{1}{2}\psi_{\tau\tau} + |\psi|^2\,\psi = 0. \tag{1}$$

This form is generally adopted to simplify the presentation of exact NLS solutions. A simple rescaling can be applied to solutions of Eq. (1) to satisfy its dimensional form

$$\mathrm{i}\left(\Psi_x + \frac{2k}{\omega}\Psi_t\right) - \frac{1}{g}\Psi_{tt} - k^3\,|\Psi|^2\,\Psi = 0. \tag{2}$$

The rescaling coefficients are straight-forward and we refer to (Kharif et al. 2009; Osborne 2010) for details. Parameters ω, k and g denote the wave number, wave frequency and gravitational acceleration, respectively. Indeed, the MI dynamics can be fully described in time and space through the family of ABs (Akhmediev et al. 1985). That is, for a given modulation frequency κ, the one parameter family of AB solutions is

$$\psi(\xi,\tau) = \exp(\mathrm{i}\xi) \times \frac{\sqrt{2\mathfrak{a}}\cos(\kappa\tau) + (1-4\mathfrak{a})\cosh(R\xi) + \mathrm{i}R\sinh(R\xi)}{\sqrt{2\mathfrak{a}}\cos(\kappa\tau) - \cosh(R\xi)}. \tag{3}$$

Here, $0 < \mathfrak{a} = \frac{1}{2} - \frac{\kappa^2}{8} < 0.5$ is the breather parameter and $R = \sqrt{8\mathfrak{a}(1-2\mathfrak{a})}$ is the growth-decay rate of AB (the same as the growth rate of MI). It is well-known that the AB solution is the exact model to study the classical MI dynamics in a deterministic framework (Wetzel et al. 2011). This dynamics has been already observed in several physical media (Dudley et al. 2009; Chabchoub et al. 2014).

Explicit analytical expressions for the second-order AB solutions can be found in Akhmediev et al. (1985), Akhmediev and Ankiewicz (1997), Akhmediev (2012). They are cumbersome and will not to be shown here. These solutions are derived using the recursive Darboux method (Akhmediev et al. 1988; Matveev and Salle 1991; Akhmediev 2012). Comprehensive description of step by step construction of AB solution of any order is given in Akhmediev et al. (1988), Akhmediev and Ankiewicz (1997). They are nonlinear superpositions of individual fundamental AB components that involve two or more eigenvalues l_i of inverse scattering technique (NLSE spectral problem). The modulation frequencies of individual components in the higher-order solutions are $\kappa_i = 2\sqrt{1+l_i^2}$ while the instability growth rate for each unstable frequency component is given by $\delta_i = \kappa_i\frac{\sqrt{4-\kappa_i^2}}{2}$. Figure 1 shows dimensional envelope propagation of the first-order AB and the higher-order AB dynamics together with their corresponding spectral evolutions, respectively.

We can clearly see in these examples that the fundamental, first-order AB describes the MI, starting from a *three wave system* (main carrier frequency and one sideband pair). For a given order n of the solution, higher-order periodic ABs initiate the instability dynamics from a $2n+1$ *wave system* (main carrier frequency and n sideband pairs). However, in present study, we will address only second-order solutions (two eigenvalue components initial five wave systems).

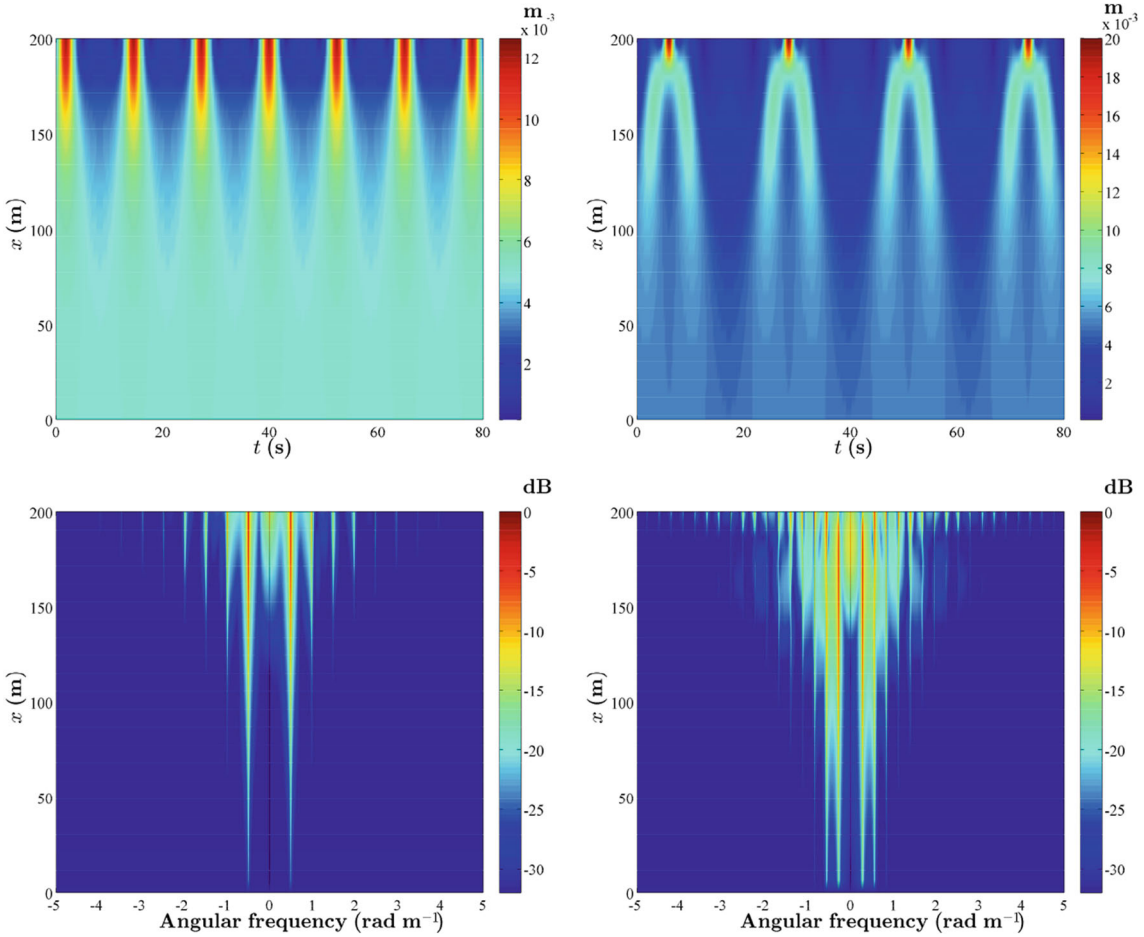

Fig. 1 *Top left* evolution of the first-order AB over 200 m for $\mathfrak{a} = 0.25$ (the case of maximal growth rate). *Top right* evolution of a second-order AB over 200 m for $\kappa_1 = 0.8$, $\delta_1 = 0.5\kappa_1\sqrt{4-\kappa_1^2}$, $\kappa_2 = 1.6$ and $\delta_2 = 0.5\kappa_2\sqrt{4-\kappa_2^2}$. The background parameters for both AB models are set to be $\varepsilon = 0.05$ and $a = 0.005$ m. *Bottom left* spectral evolution of the first-order AB. *Bottom right* spectral evolution of the higher-order AB

3 Numerical simulations and experimental set-up

The numerical two-dimensional wave tank (NWT2D) simulations are based on the boundary element method (BEM) of Tanizawa (1996) by adopting a 2.5 cm spatial resolution (see Waseda et al. 2005 for details). Laboratory experiments on AB solutions have been performed in large water wave facility, installed at The University of Tokyo, that is 50 m long and 10 m wide while the water depth is 5 m (see Mozumi et al. 2015; Waseda et al. 2015 for a photography and a schematic description). The 11 wave gauges $g_i \in [g_1, \ldots, g_{11}]$ have been placed at the following distances

$$d_i \in [d_1, \ldots, d_{11}] = [5.21, 9.00, 10.97, 14.01, 17.16, 20.15, 23.02, 25.16, 27.04, 28.91, 32.03] \quad (4)$$

To observe the water wave dynamics described by the solution of interest, $\Psi(x^*, t)$, that starts its evolution from the fixed spatial position x^*, the boundary condition applied to the flap, have to be set accordingly using the following first-order approximation for surface elevation

$$\eta(x^*, t) = \mathrm{Re}\left(\Psi(x^*, t)\exp\left[\mathrm{i}\left(kx^* - \omega t\right)\right]\right) \quad (5)$$

This is sufficient for our purpose, since the bound waves appear as soon as the wave train is generated. We also annotate that after each run, a mobile beach along the side walls have been used to damp the cross tank wave if any present.

4 Observations of the fundamental and higher-order Akhmediev breathers

In this section, we shall present the results of wave propagation on ABs with particular focus on second-order solutions, that have been so far only observed in nonlinear optical fibers (Frisquet et al. 2014).

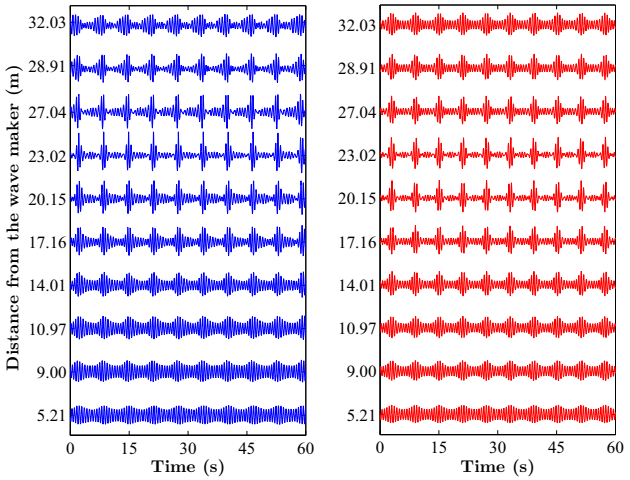

Fig. 2 *Left* AB evolution in the water wave facility for $ak = 0.10$, $a = 0.01$ m and $\mathfrak{a} = 0.25$ (*blue lines*). Corresponding NLS predictions are shown on the *right* for comparison (*red lines*)

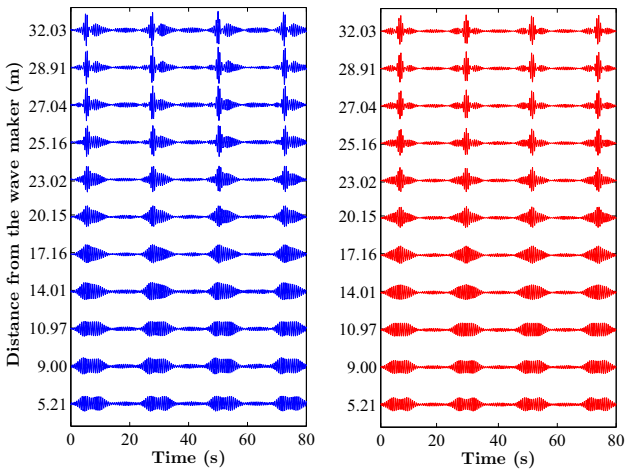

Fig. 3 *Left* higher-order Akhmediev breather observation (*blue lines*) for $\kappa_1 = 0.8$, $\delta_1 = 0.5\kappa_1\sqrt{4-\kappa_1^2}$, $\kappa_2 = 1.6$ and $\delta_2 = 0.5\kappa_2\sqrt{4-\kappa_2^2}$. The background parameters $ak = 0.05$ and $a = 0.005$ m. The corresponding theoretical NLS water surface elevation predictions to second-order of approximation are shown for comparison on the *right panel* (*red lines*)

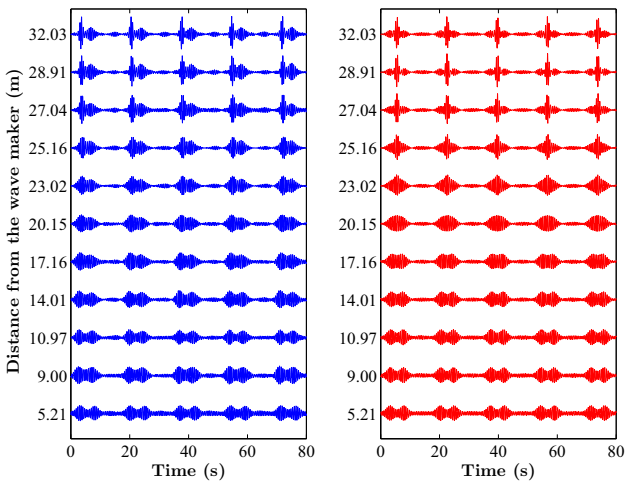

Fig. 4 *Left* higher-order Akhmediev breather observation for $\kappa_1 = 0.8$, $\delta_1 = 0.5\kappa_1\sqrt{4-\kappa_1^2}$, $\kappa_2 = 1.6$ and $\delta_2 = 0.5\kappa_2\sqrt{4-\kappa_2^2}$ (*blue lines*). The background parameters $ak = 0.06$ and $a = 0.005$ m. The corresponding theoretical NLS water surface elevation predictions to second-order of approximation are shown on the *right panel* for comparison (*red lines*)

We start showing the simplest AB-MI-model. The AB parameter is set to be $\mathfrak{a} = 0.25$, the case of maximal instability growth rate. To insure the observation of wave growth and decay in the facility we set the initial conditions at $x^* = -22$ m. Note that these ABs experience their maximal compression at $x = 0$. The propagation of the AB waves in the tank as well as the deterministic weakly nonlinear NLS forecast are shown in Fig. 2.

First, these observations show that the NLS provides a satisfactory agreement with the laboratory results for both, growth and decay processes, considering the significant wave steepness and the maximal wave amplifications reached. Furthermore, these results can be considered to be analogous to the observations of MI and the Fermi–Pasta–Ulam recurrence, starting from three wave systems, as reported in Tulin and Waseda (1999). More details can be found in Erkintalo et al. (2011), Chabchoub et al. (2014), Chabchoub and Grimshaw (2016), Kimmoun et al. (2016, 2017).

Higher-order ABs have higher amplitude amplifications than three times the background, that is the maximal amplification expected from the standard modulation instability process. Due to this fact, the steepness ak of the waves have to be decreased to avoid physical wave breaking and to allow reasonable agreement with NLS theory. Thus, the carrier parameters have been set to be $a = 0.005$ m and $ak = 0.05$ while the modulation frequency ratio is 2:1. Explicitly, $\kappa_1 = 0.8$ and $\kappa_2 = 1.6$. The evolution of this second-order AB solution for $x^* = -30$ is shown in Fig. 3.

To confirm these results, we conducted another set of experiments with a slightly higher steepness value of $ak = 0.06$. The propagation of these second-order AB-type waves with the same modulation frequency ratio, as in the previous case, is depicted in Fig. 4.

We would like to emphasize that this chosen set of parameters for the carrier and breather is dictated by the facility's dimensions and wave maker's frequency range. In both cases, the facility is too short to observe the full growth–decay cycle of such type of solutions. When the spatial co-ordinate $x^* = -30$ m is chosen to set the wave maker's initial conditions, a distance of 60 m is required to observe a quasi-Fermi–Pasta–Ulam (FPU) recurrence process. In both cases the initial envelope modulation amplitude at $x^* = -30$ m is already considerably high. This is another limitation in

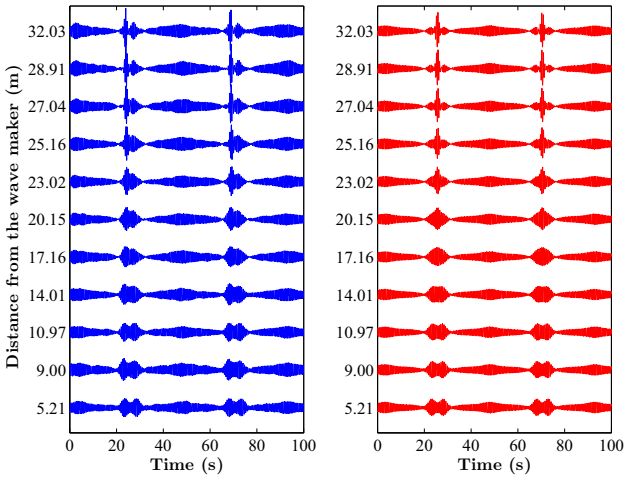

Fig. 5 *Left* higher-order Akhmediev breather observation for $\kappa_1 = 0.8$, $\delta_1 = 0.5\kappa_1\sqrt{4-\kappa_1^2}$, $\kappa_2 = 1.2$ and $\delta_2 = 0.5\kappa_2\sqrt{4-\kappa_2^2}$ (*blue lines*). The background parameters $ak = 0.05$ and $a = 0.005$ m. The corresponding NLS water surface elevation predictions to second-order of approximation are shown on the *right panel* (*red lines*)

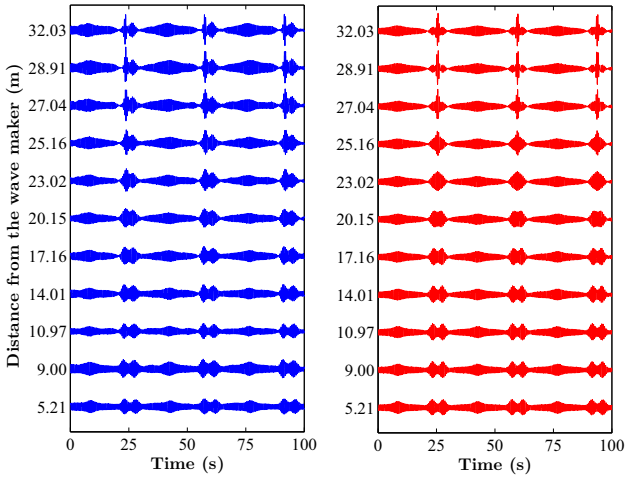

Fig. 6 *Left* higher-order Akhmediev breather observation (*blue lines*) for $\kappa_1 = 0.8$, $\delta_1 = 0.5\kappa_1\sqrt{4-\kappa_1^2}$, $\kappa_2 = 1.2$ and $\delta_2 = 0.5\kappa_2\sqrt{4-\kappa_2^2}$. The background parameters $ak = 0.06$ and $a = 0.005$ m. The corresponding theoretical NLS water surface elevation predictions to second-order of approximation are shown on the *right panel* for comparison (*red lines*)

comparing the model and experimental data. Furthermore, we observe an asymmetry of the experimental wave profiles that is due to higher-order effects, not captured in the NLS approach, see Figs. 3 and 4, and that are at play when the wave groups experience a strong nonlinear interaction and significant focusing. These are well-captured in the MNLS approach (Dysthe 1979; Trulsen and Stansberg 2001; Goullet and Choi 2011; Slunyaev et al. 2013; Chabchoub 2013; Shemer and Alperovich 2013; Chabchoub and Waseda 2016) or fully nonlinear water wave numerical schemes (Ma 2010). The asymmetry increases when the wave steepness is increased from $ak = 0.05$ to $ak = 0.06$.

In the following set of experiments we operated with the same carrier parameters, while changing the second-order ABs' modulation frequency ratio to 3:2. This is achieved by setting $\kappa_1 = 0.8$ and $\kappa_2 = 1.2$. In Fig. 5, the evolution of this breather is presented for the carrier parameters $ak = 0.05$ and $a = 0.005$ m.

As a next step, we increased the carrier parameter to $ak = 0.06$ keeping $a = 0.005$ m and observed the same type of second-order AB as before. These results are shown in Fig. 6.

When the modulation frequency ratio is 3:2, we can see clearly the obvious difference of the periodicity in the wave field compared to the case when the modulation frequency ratio is 2:1. The nonlinear wave packet interaction dynamics is also different. Generally, experimental results, shown in Figs. 5 and 6, are well-predicted by the weakly nonlinear NLS approach. As explained above, a better agreement is reached for lower steepness values. Thus, the same experimental limitations are still valid.

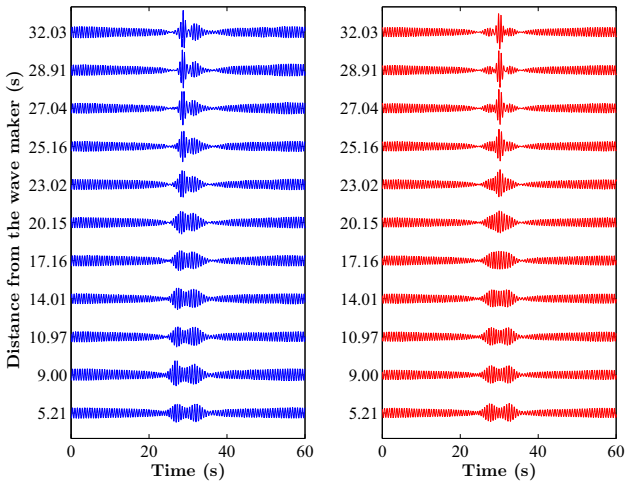

Fig. 7 *Left* degenerate higher-order Akhmediev breather observation when $\kappa = 0.8$ and $\delta = 0.5\kappa\sqrt{4-\kappa^2}$. The background parameters $ak = 0.05$ and $a = 0.005$ m (*blue lines*). *Right* the corresponding NLS water surface elevation predictions to second-order of approximation are shown on the *right panel* (*red lines*)

As a final case, we would like to discuss the case of degeneracy. This type of solutions are obtained when the imaginary eigenvalues of two ABs involved in superposition coincide (Akhmediev 2012). Namely, the limiting case of these solutions is reached when $\kappa_1 = \kappa_2$. When, additionally $\kappa_1 = \kappa_2 = 0$, this doubly-localized breather is known as the Akhmediev–Peregrine solution (Akhmediev et al. 1985, 2009a, b; Chabchoub et al. 2012; Gaillard 2015; Dontsop et al. 2016).

Figure 7 shows the excitation and evolution of the general degenerate AB case when $\kappa = \kappa_1 = \kappa_2 = 0.8$ and carrier

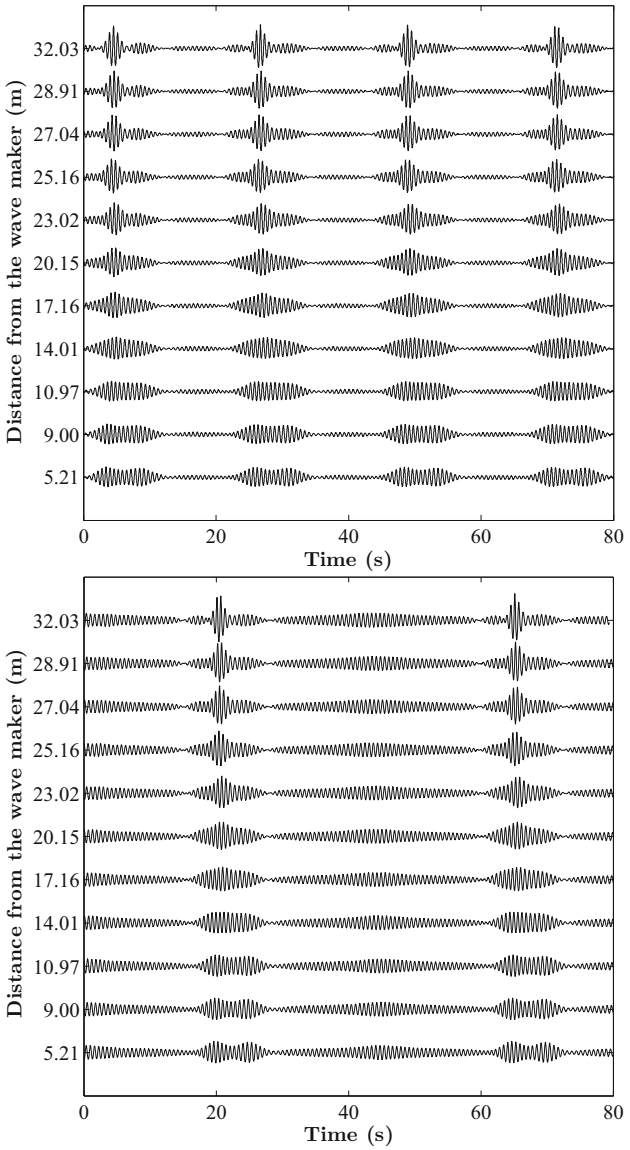

Fig. 8 NWT2D wave simulation results for $ak = 0.05$ and $a = 0.005$ (*black lines*). *Top* higher-order AB for $\kappa_1 = 0.8$ and $\kappa_2 = 1.6$. *Bottom* higher-order AB for $\kappa_1 = 0.8$ and $\kappa_2 = 1.2$

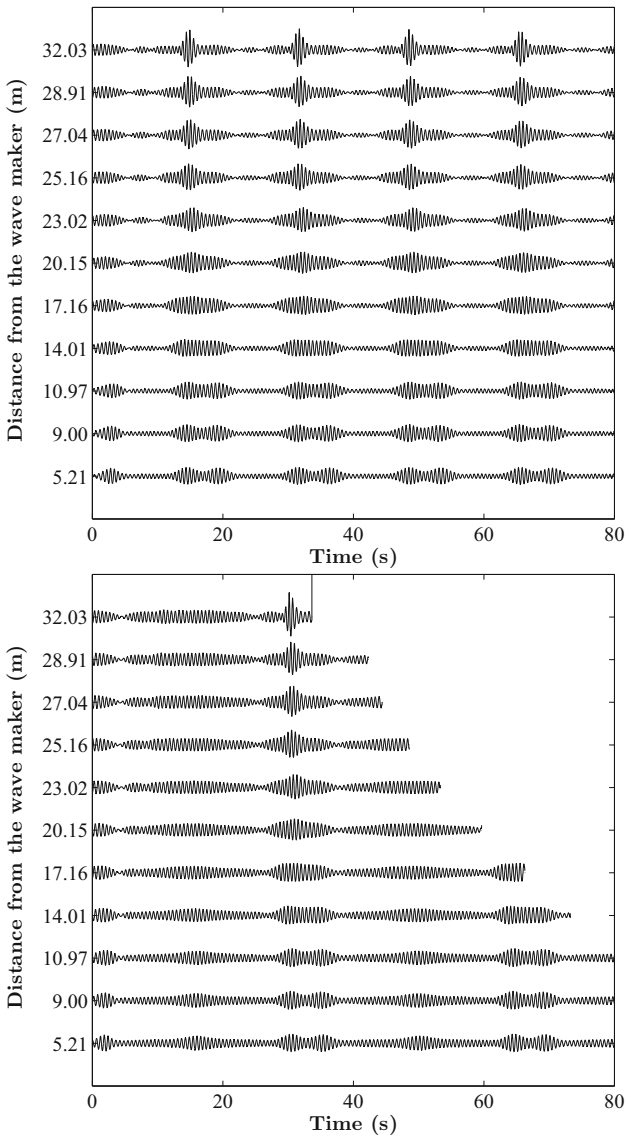

Fig. 9 NWT2D wave simulation results for $ak = 0.06$ and $a = 0.005$ (*black lines*). *Top* higher-order AB for $\kappa_1 = 0.8$ and $\kappa_2 = 1.6$. *Bottom* higher-order AB for $\kappa_1 = 0.8$ and $\kappa_2 = 1.2$

parameters $ak = 0.05$ and $a = 0.005$ m. As expected, we observe the asymmetry in the developed wave profiles which is absent in the NLS predictions. Indeed, it has been shown in Chabchoub et al. (2012) for similar type of solution and similar form of nonlinear wave interaction, a good agreement is reached when the steepness is very low (of the order of $ak = 0.03$). The major problem is that the NLS initial conditions at the starting point lead to a very steep wave evolution of Stokes waves in the experiment.

5 Results of BEM-based NWT2D simulations

In what follows, we discuss the results of the fully nonlinear BEM-based NWT2D. The spatial resolution in these simulations is 2.5 cm providing a very good accuracy for given experimental scales. This corresponds to 25 points and 20 points per wavelength for the steepness values 0.05 and 0.06, respectively. The configuration of the NWT2D simulations is identical to the wave facility in which the laboratory experiments have been performed. Namely, a plunger-type wave maker with identical dimensions is used to generate the unidirectional waves. Furthermore, a sponge layer for absorbing wave energy starts at the distance 35 m. The probes have been placed at the same positions as in the facility to capture the surface elevation data.

The data on periodic higher-order breathers have been regrouped according to their steepness. For example, Fig. 8 displays the periodic cases for the carrier steepness of $ak =$

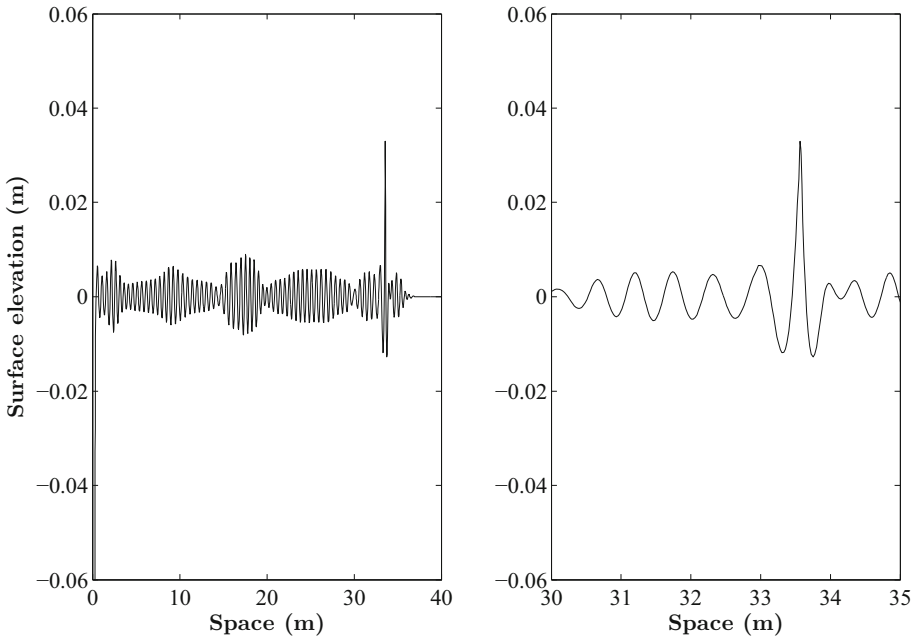

Fig. 10 (*Left*) NWT2D simulated spatial wave profile of the higher-order AB for $\kappa_1 = 0.8$ and $\kappa_2 = 1.2$ at the onset of breaking. The values $ak = 0.06$ and $a = 0.005$. (*Right*) Five meters magnification of the wave profile shown on the left near the highest amplitude point. It is also characterized by the crest slow-down (crest is slightly shifted to the *left*)

0.05. Further, the simulations of the breather cases for the steepness $ak = 0.06$ are shown together in Fig. 9. In the run for the higher-order AB for $\kappa_1 = 0.8$ and $\kappa_2 = 1.2$, the breather wave evolution led to a "blow up" of simulations. Indeed, the extreme waves, modeled by these types of breathers can be very steep and when initial carrier steepness is high, wave breaking is inevitable even at these low values of the carrier wave steepness. Interestingly, wave breaking visually was not noticed in the experiments. The wave profile in space for this latter case, one step before breaking, is shown in Fig. 10. Two different scales in Fig. 10 are used for clarity. The main feature that we can see here is the extreme amplitude peak of the wave profile in space. We can also see clearly the crest slow-down that is a particular feature of the onset of water wave breaking.

Finally, the results of simulations of degenerate case (the case for $\kappa = 0$) are shown in Fig. 11. The dynamics of the wave profile here is very similar to the Akhmediev–Peregrine solution. Indeed, the extreme wave (at $x = 0$) emerges from the nonlinear superposition of the two modulated wave envelopes (Chabchoub et al. 2012). However, the maximal wave amplitude reached in this evolution is smaller than the theoretical limiting Akhmediev–Peregrine value that is five, see (Akhmediev 2012).

Generally, all the NWT2D simulations show an excellent agreement with laboratory experiments, as they use the fully-nonlinear governing water wave equations for an idealized fluid (Liggett and Liu 1984; Yeung 1982). In fact, the wave features in them are almost identical. These are: focusing evolution in time and space, wave packet's asymmetry as well as the group velocity. This fact demonstrates the efficiency of

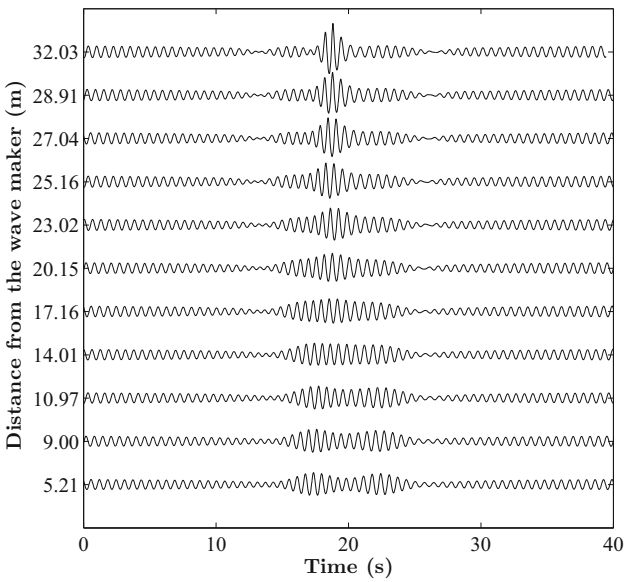

Fig. 11 NWT2D wave measurement results of the degenerate higher-order AB for $ak = 0.05$ and $a = 0.005$ as well as $\kappa = 0.8$ (*black lines*)

the NWT2D numerical model in simulating hydrodynamic extremes. It has stronger potential for applications in ocean and naval engineering, compared to other nonlinear numerical schemes (Ma 2010).

6 Discussion

In this Section, we compare the wave dynamics of higher-order ABs obtained in laboratory observations with theoret-

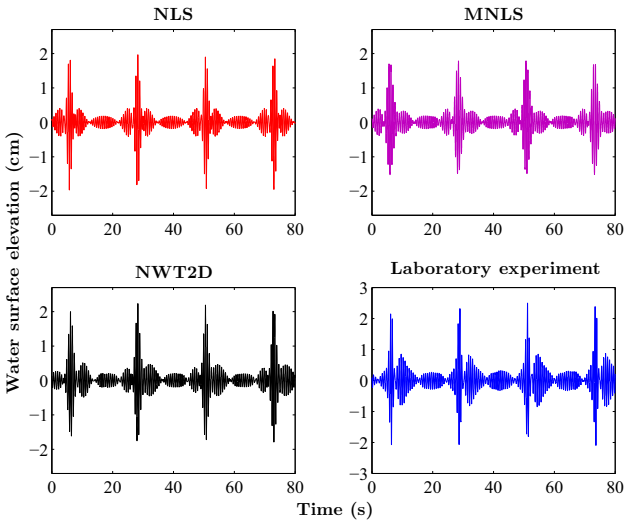

Fig. 12 Comparison of experimental data with theory and simulations for the focused higher-order AB water surface elevations for the case: $\kappa_1 = 0.8, \kappa_2 = 1.6, ak = 0.05$ and $a = 0.005$ m. *Top left* Theory within the NLS framework (*red lines*), Top Right: MNLS simulations (*purple lines*), *Bottom left* NWT2D simulations (black lines) and *Bottom right* Laboratory data (*blue lines*)

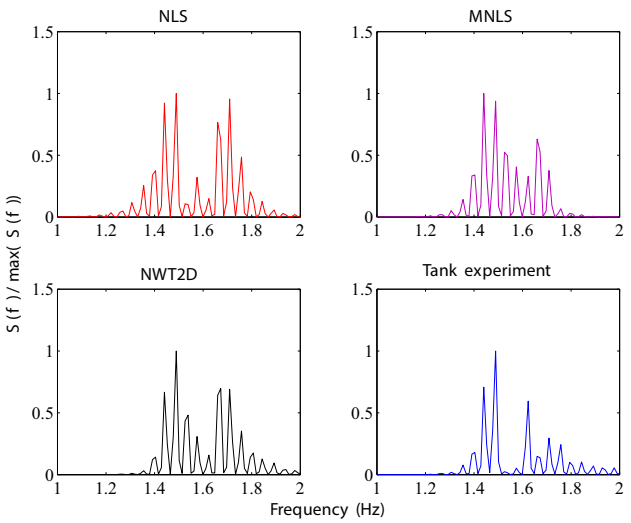

Fig. 13 The spectra of the water surface elevations for the same set of data as in Fig. 12

ical NLS framework, with NWT2D simulations as well as with the MNLS. The latter extension of the NLS is known to take into account higher-order dispersion and the mean flow of the wave field (Dysthe 1979; Trulsen and Stansberg 2001; Goullet and Choi 2011). For the sake of brevity, we make the comparison only for the case shown in Fig. 2. Namely, for the case of the higher-order AB solution with $\kappa_1 = 0.8$ and $\kappa_2 = 1.6$ and for the carrier parameters $ak = 0.05$ and $a = 0.005$ m. Figure 12 shows the results of the comparison.

The NLS predicts well the wave focusing and its major parameters such as the amplitude amplification and shape of the wave packet. Naturally, the MNLS simulations are in a better agreement with experimental data. This can be expected considering the physical limitations of the NLS as well as the significant amplifications reached in experiment (Trulsen and Stansberg 2001; Chabchoub 2013; Slunyaev et al. 2013; Shemer and Alperovich 2013). However, the best agreement is reached when the BEM-based NWT2D simulations are used with the chosen resolution of 2.5 cm. These results show a striking agreement with the laboratory data. The agreement is completed with the asymmetry of the focused wave packets as well as extreme wave heights. A good agreement is also observed in the spectral domain as shown in Fig. 13.

Even though the BEM-NWT2D seems to be the most accurate framework in describing the very steep waves, the computation time was much longer compared to NLS or MNLS simulations. However, this technique is very useful for studies involving more complete physical properties of the wave field beyond extracting simple water surface elevations.

7 Conclusions

We have reported observations of higher-order AB dynamics in a water wave facility. These include periodic second-order ABs with two different modulation frequencies and degenerate AB when the frequencies coincide. The steepness values have been set to be relatively small to stay within the limits of NLS theory. As a direct consequence of these limitations, the propagation distance in the facility was not sufficient to allow the observation of the full growth–decay cycle (known as Fermi–Pasta–Ulam recurrence) of these pulsating localized structures. The experiments are in a very good agreement with the fully nonlinear BEM-based NWT2D simulations with a spatial resolution of 2.5 cm while NLS provides a solid predicting power to study these higher-order breathers in a given hydrodynamic environment. Future work will be devoted to studies of the limitations of the theory of higher-order ABs when applied to the water surface as well as their applicability to realistic oceanic conditions following an example of Chabchoub (2016). Furthermore, the choice of NWT2D resolution in the analysis of steep nonlinear waves needs further investigations.

Acknowledgements A.C. acknowledges the support from the Japan Society for the Promotion of Science (JSPS) and the Burgundy Region (France). A.C. and T.W. acknowledges the support from the Japan Society for the Promotion of Science (JSPS) through Grants-in-Aid for Scientific Research (KAKENHI). B.K. is thankful for support from French project PIA2/ISITE-BFC. N.A. acknowledges the support of the Australian Research Council (Discovery Project numbers DP140100265 and DP150102057) and support from the Volkswagen Stiftung.

References

Akhmediev N, Ankiewicz A (1997) Solitons: nonlinear pulses and beams. Chapman & Hall, London

Akhmediev N, Ankiewicz A, Soto-Crespo J (2009) Rogue waves and rational solutions of the nonlinear Schrödinger equation. Phys Rev E 80(2):026601

Akhmediev N, Ankiewicz A, Taki M (2009) Waves that appear from nowhere and disappear without a trace. Phys Lett A 373(6):675–678

Akhmediev N, Eleonskii VM, Kulagin NE (1985) Generation of periodic trains of picosecond pulses in an optical fiber: exact solutions. Sov Phys JETP 62(5):894–899

Akhmediev N, Eleonskii VM, Kulagin NE (1987) Exact solutions of the first order of nonlinear Schrödinger equation. Theor Math Phys (USSR) 72(2):809–818

Akhmediev N, Korneev VI (1986) Modulation instability and periodic solutions of the nonlinear Schrödinger equation. Theor Math Phys (USSR) 69(2):1089–1093

Akhmediev N, Korneev V, Mitskevich N (1988) N-modulation signals in a single-mode optical waveguide under nonlinear conditions. Zh Eksp Teor Fiz 94:159–170

Benjamin TB, Feir J (1967) The disintegration of wave trains on deep water part 1. Theory. J Fluid Mech 27(03):417–430

Benjamin TB, Hasselmann K (1967) Instability of periodic wavetrains in nonlinear dispersive systems (and discussion). In: Proceedings of the Royal Society of London A: Mathematical, Physical and Engineering Sciences, vol 299, The Royal Society, pp 59–76

Bitner-Gregersen EM, Gramstad O (2015) Rogue waves impact on ships and offshore structures. DNV-GL

Chabchoub A (2016) Tracking breather dynamics in irregular sea state conditions. Phys Rev Lett 117(14):144103

Chabchoub A, Grimshaw RH (2016) The hydrodynamic nonlinear Schrödinger equation: space and time. Fluids 1(3):23

Chabchoub A, Hoffmann N, Akhmediev N (2011) Rogue wave observation in a water wave tank. Phys Rev Lett 106(20):204502

Chabchoub A, Hoffmann N, Onorato M, Akhmediev N (2012) Super rogue waves: observation of a higher-order breather in water waves. Phys Rev X 2(1):011015

Chabchoub A, Hoffmann N, Onorato M, Genty G, Dudley JM, Akhmediev N (2013) Hydrodynamic supercontinuum. Phys Rev Lett 111(5):054104

Chabchoub A, Kibler B, Dudley J, Akhmediev N (2014) Hydrodynamics of periodic breathers. Philos Trans R Soc Lond A Math Phys Eng Sci 372(2027):20140005

Chabchoub A, Waseda T (2016) Modulation instability and extreme events beyond initial three wave systems. In: ASME 2016 35th international conference on ocean, offshore and arctic engineering, American Society of Mechanical Engineers, pp V003T02A036–V003T02A036

Dontsop PYG, Essama BGO, Dongo JM, Dedzo MM, Atangana J, Yemele D, Kofane TC (2016) Akhmediev–Peregrine rogue waves generation in a composite right/left-handed transmission line. Opt Quant Electron 48:59

Dudley JM, Genty G, Dias F, Kibler B, Akhmediev N (2009) Modulation instability, Akhmediev breathers and continuous wave supercontinuum generation. Opt Express 17(24):21497–21508

Dysthe KB (1979) Note on a modification to the nonlinear Schrödinger equation for application to deep water waves. In: Proceedings of Royal Society of London A: Mathematical, Physical and Engineering Sciences, The Royal Society, vol 369, pp 105–114

Erkintalo M, Genty G, Wetzel B, Dudley JM (2011) Akhmediev breather evolution in optical fiber for realistic initial conditions. Phys Lett A 375(19):2029–2034

Frisquet B, Chabchoub A, Fatome J, Finot C, Kibler B, Millot G et al (2014) Two-stage linear-nonlinear shaping of an optical frequency comb as rogue nonlinear-Schrödinger-equation-solution generator. Phys Rev A 89(2):023821

Gaillard P (2015) Other $2N-2$ parameters solutions of the NLS equation and 2N + 1 highest amplitude of the modulus of the N-th order Akhmediev-Peregrine breather. J Phys A Math Theor 48:145203

Goullet A, Choi W (2011) A numerical and experimental study on the nonlinear evolution of long-crested irregular waves. Phys Fluids 23(1):016601

Kedziora DJ, Ankiewicz A, Akhmediev N (2012) Second-order nonlinear Schrödinger equation breather solutions in the degenerate and rogue wave limits. Phys Rev E 85:066601

Kharif C, Pelinovsky E (2003) Physical mechanisms of the rogue wave phenomenon. Eur J Mech B Fluids 22(6):603–634

Kharif C, Pelinovsky E, Slunyaev A (2009) Rogue waves in the ocean. Springer, New York

Kibler B, Chabchoub A, Gelash A, Akhmediev N, Zakharov VE (2015) Superregular breathers in optics and hydrodynamics: omnipresent modulation instability beyond simple periodicity. Phys Rev X 5(4):041026

Kibler B, Fatome J, Finot C, Millot G, Dias F, Genty G, Akhmediev N, Dudley JM (2010) The Peregrine soliton in nonlinear fibre optics. Nat Phys 6(10):790–795

Kimmoun O, Hsu H, Branger H, Li M, Chen Y, Kharif C, Onorato M, Kelleher E, Kibler B, Akhmediev N et al (2016) Modulation instability and phase-shifted Fermi-Pasta-Ulam recurrence. Sci Rep 6:28516

Kimmoun O, Hsu H, Kibler B, Chabchoub A (2017) Nonconservative higher-order hydrodynamic modulation instability. Phys Rev E 96:022219

Liggett J, Liu P-F (1984) Applications of boundary element methods to fluid mechanics. In: Basic principles and applications, Springer, New York, pp 78–96

Ma Q (2010) Advances in numerical simulation of nonlinear water waves, vol 11. World Scientific, Singapore

Matveev VB, Salle MA (1991) Darboux transformations and solitons. Springer, New York

Mozumi K, Waseda T, Chabchoub A (2015) 3D stereo imaging of abnormal waves in a wave basin. In: ASME 2015 34th International conference on ocean, offshore and arctic engineering, American Society of Mechanical Engineers, pp V003T02A027–V003T02A027

Onorato M, Proment D, Clauss G, Klein M (2013) Rogue waves: from nonlinear Schrödinger breather solutions to sea-keeping test. PLoS One 8(2):e54629

Osborne A (2010) Nonlinear ocean waves and the inverse scattering transform, vol 97. Academic Press, Cambridge

Shemer L, Alperovich L (2013) Peregrine breather revisited. Phys Fluids (1994-present) 25(5):051701

Slunyaev A, Pelinovsky E, Sergeeva A, Chabchoub A, Hoffmann N, Onorato M, Akhmediev N (2013) Super-rogue waves in simulations based on weakly nonlinear and fully nonlinear hydrodynamic equations. Phys Rev E 88(1):012909

Tai K, Hasegawa A, Tomita A (1986) Observation of modulational instability in optical fibers. Phys Rev Lett 56(2):135

Tanizawa K (1996) Long time fully nonlinear simulation of floating body motions with artificial damping zone. J Soc Naval Arch Jpn 180:311–319

Trulsen K, Stansberg CT (2001) Spatial evolution of water surface waves: numerical simulation and experiment of bichromatic waves. In: Proceedings of the eleventh international offshore and polar engineering conference, Stavanger, Norway, 17–22 June 2017

Tulin MP, Waseda T (1999) Laboratory observations of wave group evolution, including breaking effects. J Fluid Mech 378:197–232

Waseda T, Kinoshita T, Cavaleri L, Toffoli A (2015) Third-order resonant wave interactions under the influence of background current fields. J Fluid Mech 784:51–73

Waseda T, Rheem C-K, Sawamura J, Yuhara T, Kinoshita T, Tanizawa K, Tomita H et al (2005) Extreme wave generation in laboratory wave tank. In: Proceedings of the fifteenth international offshore and polar engineering conference, Seoul, Korea, 19–24 June 2005

Wetzel B, Erkintalo M, Genty G, Hammani K, Kibler B, Fatome J, Finot C, Dias F, Akhmediev N, Millot G et al (2011) New analysis of an old instability. Optoelectron Commun SPIE Newsroom 10:2–1201104

Yeung RW (1982) Numerical methods in free-surface flows. Annu Rev Fluid Mech 14(1):395–442

Zakharov VE (1968) Stability of periodic waves of finite amplitude on the surface of a deep fluid. J Appl Mech Technol Phys 9(2):190–194

Zakharov VE, Ostrovsky LA (2009) Modulation instability: the beginning. Physica D 238(5):540–548